Journal of Biomedical Optics

SPIEDigitalLibrary.org/jbo

Label-free photoacoustic microscopy of myocardial sheet architecture

Chi Zhang
Ya-Jian Cheng
Junjie Chen
Samuel Wickline
Lihong V. Wang

SPIE

Label-free photoacoustic microscopy of myocardial sheet architecture

Chi Zhang,[a] Ya-Jian Cheng,[b] Junjie Chen,[b] Samuel Wickline,[b] and Lihong V. Wang[a]
[a]Washington University in St. Louis, Department of Biomedical Engineering, Optical Imaging Laboratory, One Brookings Drive, St. Louis, Missouri 63130
[b]Washington University School of Medicine, Cardiovascular Division, Campus Box 8215, 4320 Forest Park Avenue, St. Louis, Missouri 63108

Abstract. Cardiac myofibers are organized into sheet architectures, which contribute to up to 40% of the heart wall thickening for ejection of blood for circulation. It is important to delineate the sheet architecture for a better understanding of cardiac mechanisms. However, current sheet imaging technologies are limited by fixation-induced dehydration/deformation and low spatial resolution. Here we implemented high-resolution label-free photoacoustic microscopy (PAM) of the myocardial sheet architecture. With high endogenous optical-absorption contrast originating mainly from cytochrome, myoglobin, and melanin, PAM can image the unfixed, unstained and unsliced heart without introducing deformation artifacts. A fresh blood-free mouse heart was imaged by PAM *ex vivo*. The three-dimensional branching sheets were clearly identified within 150 μm depth. Various morphological parameters were derived from the PAM image. The sheet thickness (80 ± 10 μm) and the cleavage height (11 ± 1 μm) were derived from an undehydrated heart for the first time. Therefore, PAM has the potential for the functional imaging of sheet architecture in *ex vivo* perfused and viable hearts. [DOI: 10.1117/1.JBO.17.6.060506]

Keywords: photoacoustic microscopy; myocardial sheet architecture; label-free; undehydrated.

Paper 12186L received Mar. 18, 2012; revised manuscript received May 3, 2012; accepted for publication May 8, 2012; published online Jun. 6, 2012.

The heart comprises a syncytium of cardiomyocytes that are important for optimizing cardiac functions through coordinated excitation-contraction-relaxation cycles.[1] Delineating the exact myocardial architecture is critical to understanding the exact mechanisms of cardiac functions, such as the wall thickening and the ventricular longitudinal shortening. Recently, myocardial fibers have been found to be organized in branching layers separated by cleavages, referred to as the "sheet architecture".[1–3] It has been reported that the systolic wall shear aligns along the sheet direction,[1] and the myocardial sheet is the major infrastructure contributing to systolic wall thickening for ejection of blood.[4,5] However, the exact three-dimensional (3-D) complex sheet architecture remains to be defined for a better understanding of cardiac mechanisms.

One of the difficulties in studying myocardial sheet architecture is the lack of appropriate imaging technologies. Histology is the traditional method to image the myocardial architectures. However, the fixation and slicing procedures inevitably deform the native sheet architecture, resulting in unnatural morphology. Confocal optical microscopy has been used to image the surface of a block of fixed heart tissue.[2] The deeper part of the tissue can be imaged by repeatedly removing thin layers of the surface. Although, the deformation induced by slicing can be avoided by this technique, the tissue still requires fixation and staining, which dehydrate and deform the native sheet architecture. Diffusion-tensor MRI can delineate the sheet architecture nondestructively in viable hearts;[4,6] however, it cannot provide micrometer-level resolution within applicable scan times of less than one day per sample. Therefore, a fast high-resolution imaging technology is still required for visualizing the myocardial sheets in unfixed and unstained, and thereby undeformed hearts.

Photoacoustic microscopy (PAM) is suitable for imaging the myocardial sheet architecture for the following reasons. First, PAM can achieve submicrometer transverse resolution in the optical ballistic regime (~1 mm deep),[7,8] and can also work in the optical diffusive regime (up to several centimeters deep) at acoustic resolution.[9] PAM with scalable resolution and depth can provide consistent studies of the sheet architecture in hearts on various scales. Second, PAM can detect endogenous optical-absorption contrast with a 100% sensitivity without labeling the tissue.[10] Cytochrome, myoglobin, and melanin have been reported as the endogenous light-absorbing sources in myocytes,[11–13] and are expected to be the origins of signals for label-free PAM of myocardium. Therefore, in this pilot study, we implemented label-free PAM of myocardial sheet architecture for the first time.

Optical-resolution PAM was used to image myocardial sheet architecture, as demonstrated in Fig. 1. For spectral measurement, we used an integrated diode-pumped Q-switched laser and optical parametric oscillator system (NT242-SH, Ekspla) with a wavelength tunable from 210 to 2600 nm and a pulse repetition rate of 1 KHz.[14] For fast imaging, we used a Nd:YVO4 laser (SPOT 10-200-532, Elforlight), which provides a repetition rate up to 50 KHz but a fixed wavelength of 532 nm.[7] The details of the optical parts of the system can be found in Refs. 7 and 14. The laser pulses were focused by an optical objective (0.32 numerical aperture) to the heart muscle. The excited photoacoustic waves were detected by an ultrasonic transducer (40 MHz central frequency, 80% bandwidth), and their amplitudes were proportional to the optical absorption density at the optical foci. Mapping of the optical absorption in 3-D was achieved by 2-D raster scanning while the depth was converted from the arrival time of the photoacoustic signals from each scanning point. Here the transverse resolution was ~0.8 μm (at 532 nm wavelength), and the axial resolution enhanced by deconvolution[8] was ~15 μm.

The origins of optical absorption in heart muscles were measured quantitatively by photoacoustic spectroscopy. A mouse (Hsd:ND4, Harlan Co.) heart was saline-perfused (to wash out blood and avoid strong signals from hemoglobin), excised, and formalin-fixed. We used PAM to measure the average signal

Address all correspondence to: Lihong V. Wang, Washington University in St. Louis, Department of Biomedical Engineering, Optical Imaging Laboratory, One Brookings Drive, St. Louis, Missouri 63130. Tel: (314) 935-6152; Fax: (314) 935-7448; E-mail: lhwang@biomed.wustl.edu

0091-3286/2012/$25.00

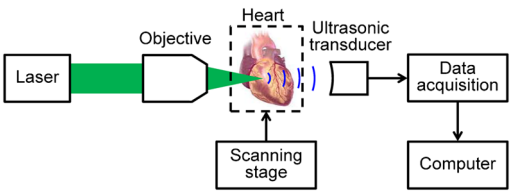

Fig. 1 Schematic of the PAM system.

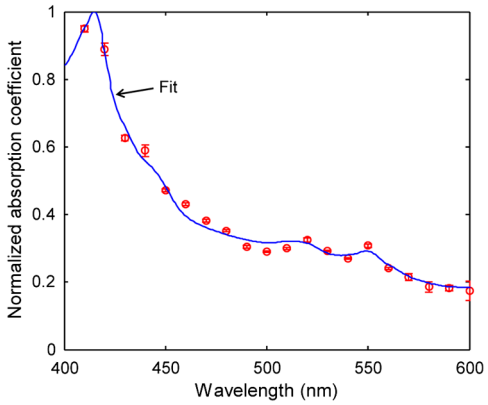

Fig. 2 Spectra of the absorption coefficient of the blood-free mouse myocardium: PAM measurement (circles) and fit with the sum of reduced cytochrome *c*, melanin, and metmyoglobin (line).

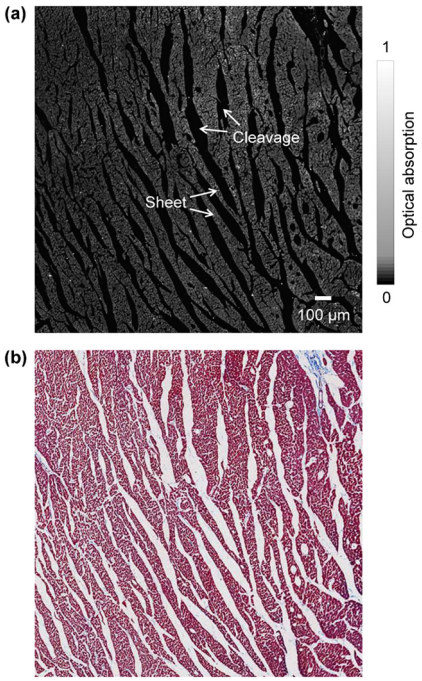

Fig. 3 Imaging of a histological section of a dog heart in the left ventricular wall region with and without labeling. (a) Label-free PAM image. (b) Bright-field optical microscopy image with Masson's trichrome staining.

amplitude (normalized by the laser pulse energy) from the left ventricular myocardium within the wavelength range of 400 to 600 nm, as shown in Fig. 2. In the absence of hemoglobin, the main absorbers in myocardium are expected to be formalin-reduced cytochrome *c*,[15] melanin, and metmyoglobin which accumulates in dead muscles.[11–13] The PAM data can be fitted with a linear combination of the molar absorption spectra of the main absorbers to quantify the relative concentrations of the constituents, as depicted in Eq. (1) and Fig. 2,[16]

$$\phi(\lambda) \propto \varepsilon_{\mathrm{cyt}}(\lambda)C_{\mathrm{cyt}} + \varepsilon_{\mathrm{mel}}(\lambda)C_{\mathrm{mel}} + \varepsilon_{\mathrm{myo}}(\lambda)C_{\mathrm{myo}}, \quad (1)$$

where $\phi(\lambda)$ is the wavelength-dependent photoacoustic signal amplitude; $\varepsilon_{\mathrm{cyt}}(\lambda)$, $\varepsilon_{\mathrm{mel}}(\lambda)$, and $\varepsilon_{\mathrm{myo}}(\lambda)$ are the wavelength-dependent molar extinction coefficients of reduced cytochrome *c*, melanin, and metmyoglobin, respectively; C_{cyt}, C_{mel}, and C_{myo} are the molar concentrations of reduced cytochrome *c*, melanin, and metmyoglobin, respectively. C_{cyt}, C_{mel}, and C_{myo} can be calculated in relative values by Eq. (1). The mass ratio was converted from the molar ratio for the formalin-fixed mouse heart sample, with a resulting ratio of reduced cytochrome *c* to melanin to metmyoglobin of 6.1:3.7:1 with a coefficient of determination (R^2) of 0.993. The accuracy of this result, however, is subject to the possible presence of other neglected absorbers such as oxidized cytochrome *c*, oxy-/deoxy-myoglobin, and lipofuscin.

We imaged a histological section of a blood-free paraffin-embedded dog heart. The unstained section in the left ventricular wall area was imaged by PAM with ~50 nJ pulse energy. As shown in Fig. 3(a), the myocardial sheets and sheet cleavages can be identified clearly with a contrast-to-noise ratio (CNR) of 41 dB between the two tissue components. These unstained structures are nearly invisible with bright-field optical microscopy due to the extremely low CNR of 4.6 dB (not shown here). The bright-field image with Masson's trichrome staining is shown in Fig. 3(b). The two images match well with a correlation coefficient of 0.91 when both images were thresholded at 3 times of the corresponding noise levels. Therefore, PAM can sensitively detect the endogenous absorption in myocardium with a fine resolution to resolve the sheet architecture. Moreover, it can be seen in Fig. 3 that the sheet architecture is deformed (e.g., the cleavage height becomes much larger than usual) due to dehydration and slicing.

With high endogenous contrast, PAM was investigated to image the unstained and unsliced heart without introducing deformation artifacts. A saline-perfused blood-free heart of a mouse (Hsd:ND4, Harlan Co.) was excised and then imaged by PAM *ex vivo* with ~80 nJ pulse energy. The heart was split into halves as shown in Fig. 4(a), but it was unfixed and unstained and thereby undeformed. The myocardium in the left ventricular free wall, indicated by the square region in Fig. 4(a), was imaged by PAM. Figure 4(b) shows the PAM image in maximum amplitude projection along the depth direction from 20 to 50 μm. A close-up of the marked region in Fig. 4(b) is shown in Fig. 4(c), where the branching sheets can be clearly identified with a CNR of 36 dB. Two populations of oppositely signed sheet angles were observed. The boundaries of the sheets were extracted, and the long axis from the apex to the base of the heart is marked in Fig. 4(c). Various morphological parameters can be calculated from this image. The average angle between the sheet and the ventricular short axis is 30 ± 2 deg, in agreement with previously reported data.[4] The average sheet thickness is 80 ± 10 μm, and the average cleavage height is 11 ± 1 μm, both parameters being reported for the first time in an undehydrated heart, to the best of our knowledge.

The 3-D sheet architecture of the same heart is shown by Fig. 5. The heart was scanned twice, focusing at 40 and 100 μm depth, respectively. Figure 5 shows the movies of 3-D image

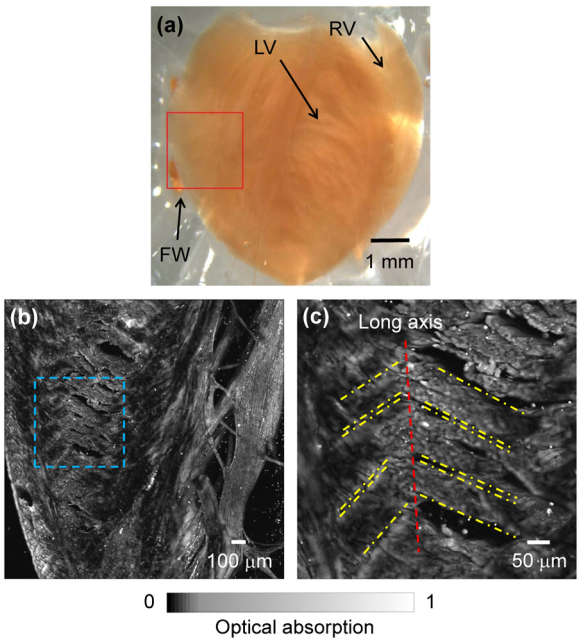

Fig. 4 Imaging of a blood-free half-split mouse heart, unfixed and unstained. (a) Photograph of the heart: LV, left ventricle; RV, right ventricle; FW, free wall. (b) PAM image of the FW region marked in (a) acquired at 532-nm wavelength. (c) Close-up PAM image of the marked region in (b). The boundaries of the branching sheets are extracted: long axis (red dashed line) and sheet boundaries (yellow dashed-dot line).

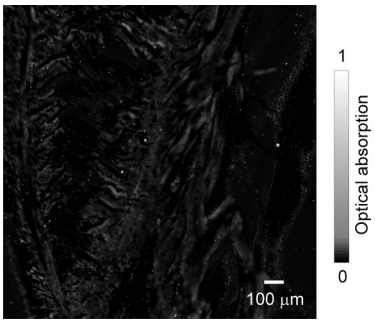

Fig. 5 Movies of 3-D image stacks in the same area as Fig. 4(b) down to 150 μm in depth. The movies shown by multimedia files Video 1 (MPEG, 5.1 MB) [http://dx.doi.org/10.1117/1.JBO.17.6.060506.1], Video 2 (MPEG, 5.6 MB) [http://dx.doi.org/10.1117/1.JBO.17.6.060506.2], and Video 3 (MPEG, 5.6 MB) [http://dx.doi.org/10.1117/1.JBO.17.6.060506.3] scan through the myocardium in three directions.

stacks in the same area as Fig. 4(b) down to 150 μm in depth. The movies scan through the myocardium in three directions for 3-D visualization of sheet development. As shown by the movies, PAM can delineate the accurate 3-D myocardial structure in unfixed and unstained hearts.

Here the PAM image of the heart muscle was obscured beyond the depth of 150 μm, so the heart was split into halves in order to reveal the 3-D sheet architecture. To show the sheet architecture in an intact mouse heart, we need a penetration depth of ~1 mm, which is nearly the penetration limit of optical-resolution PAM. Near-infrared illumination and acoustic-resolution PAM[9] (with a >200 MHz ultrasonic transducer for fine lateral resolution) can be used for the 1 mm or deeper penetration in future studies. Moreover, by further enhancing the axial resolution and the imaging speed, we expect to develop PAM for accessing dynamic changes of myocardial architectures in *ex vivo* perfused and viable hearts. The heart can be arrested in diastole and systole in sequence, during which the heart is imaged by PAM. The functional role of the myocardial sheets can then be analyzed.

In summary, we have realized label-free PAM of myocardial sheet architecture in the undeformed mouse heart *ex vivo*. The sheet thickness and the cleavage height in an undehydrated heart are reported for the first time. We expect to further develop PAM for the functional imaging of sheet architecture in *ex vivo* perfused and viable hearts.

Acknowledgments

The authors thank Dr. Igor Efimov for providing the dog heart sections and Dr. Da-Kang Yao for experimental assistance. This work was sponsored in part by National Institutes of Health (NIH) grants R01 EB000712, R01 EB008085, R01 CA134539, U54 CA136398, R01 CA157277, and R01 CA159959. L.W. has a financial interest in Microphotoacoustics, Inc. and Endra, Inc., which, however, did not support this work.

References

1. K. D. Costa et al., "Laminar fiber architecture and three-dimensional systolic mechanics in canine ventricular myocardium," *Am. J. Physiol. Heart Circ. Physiol.* **276**(2), H595–H607 (1999).
2. A. J. Pope et al., "Three-dimensional transmural organization of perimysial collagen in the heart," *Am. J. Physiol. Heart Circ. Physiol.* **295**(3), H1243–H1252 (2008).
3. I. J. LeGrice et al., "Laminar structure of the heart: ventricular myocyte arrangement and connective tissue architecture in the dog," *Am. J. Physiol. Heart Circ. Physiol.* **269**(2), H571–H582 (1995).
4. J. Chen et al., "Regional ventricular wall thickening reflects changes in cardiac fiber and sheet structure during contraction: quantification with diffusion tensor MRI," *Am. J. Physiol. Heart Circ. Physiol.* **289**(5), H1898–H1907 (2005).
5. I. J. LeGrice, Y. Takayama, and J. W. Covell, "Transverse shear along myocardial cleavage planes provides a mechanism for normal systolic wall thickening," *Circ. Res.* **77**(1), 182–193 (1995).
6. D. F. Scollan et al., "Histological validation of myocardial microstructure obtained from diffusion tensor magnetic resonance imaging," *Am. J. Physiol. Heart Circ. Physiol.* **275**(6), H2308–H2318 (1998).
7. C. Zhang, K. Maslov, and L. V. Wang, "Subwavelength-resolution label-free photoacoustic microscopy of optical absorption in vivo," *Opt. Lett.* **35**(19), 3195–3197 (2010).
8. C. Zhang et al., "Reflection-mode submicron-resolution in vivo photoacoustic microscopy," *J. Biomed. Opt.* **17**(2), 020501 (2012).
9. H. F. Zhang et al., "Functional photoacoustic microscopy for high-resolution and noninvasive in vivo imaging," *Nat. Biotech.* **24**(7), 848–851 (2006).
10. L. V. Wang, "Multiscale photoacoustic microscopy and computed tomography," *Nat. Photon.* **3**(9), 503–509 (2009).
11. A. E. Arai et al., "Myocardial oxygenation in vivo: optical spectroscopy of cytoplasmic myoglobin and mitochondrial cytochromes," *Am. J. Physiol. Heart Circ. Physiol.* **277**(2), H683–H697 (1999).
12. D. H. Dolley and F. V. Guthrie, "The pigmentation of heart muscle," *J. Med. Res.* **42**(3), 289–301 (1921).
13. G. Majno and I. Joris, *Cells, Tissues, and Disease: Principles of General Pathology*, pp. 107–108, Oxford University Press, Oxford, New York (2004).
14. C. Zhang et al., "Label-free photoacoustic microscopy of cytochrome *c* in cells," *J. Biomed. Opt.*, submitted.
15. C. Anthony, "Cytochrome c and the oxidation of C_1 compounds in Pseudomonas AM 1," *Biochem. J.* **119**(5), 54P–55P (1970).
16. J. Laufer et al., "Quantitative spatially resolved measurement of tissue chromophore concentrations using photoacoustic spectroscopy: application to the measurement of blood oxygenation and haemoglobin concentration," *Phys. Med. Biol.* **52**(1), 141–168 (2007).